18. Y. Jenkins and J. K. Barton, *J. Am. Chem. Soc.* **114**, 8736 (1992). Association of the tethered metal complex with single-stranded DNA may lead to anomalous luminescent behavior; thus careful annealing is required.
19. $Rh(phi)_2phen'^{3+}$ can be prepared in a manner analogous to that for the parent phenanthroline complex (*16*).
20. 5′-d(AGTGCCAAGCTTGCA)-3′ and its complement were synthesized on an Applied Biosystems 394 DNA synthesizer and modified at the 5′ end with the reagent Aminolink2 (A.B.I.), which yields a 5′-NH_2-$(CH_2)_6$-OPO_3–terminus. Coupling the metal complexes to the amino-DNA has been accomplished with 1-hydroxybenzotriazole and dicyclohexylcarbodiimide in a 1:1 dimethylformamide:dioxane slurry (*18*). Products were separated by high-performance liquid chromatography on a Hewlett-Packard 1050 system with a C_{18} column (Vydac) and a triethylamine–acetic acid/acetonitrile gradient. Yields were poor (1% at best). Metal complex content was established by ultraviolet-visible spectroscopy, and DNA content was determined by an analytical test for phosphate [O. Lindberg and L. Ernsten, *Methods of Biochemical Analysis*, D. Glick, Ed. (Interscience: New York, 1954), vol. 3].
21. For other examples of the tethering of metal-phenanthroline complexes to oligonucleotides, see W. Bannwarth, D. Schmidt, R. L. Stallard, C. Hornung, and R. Knorr [*Helv. Chim. Acta* **71**, 2085 (1988)]; J. Telser, K. A. Cruickshank, K. S. Schanze, and T. L. Netzel [*J. Am. Chem. Soc.* **111**, 7221 (1989)]; and C. H. B. Chen and D. S. Sigman [*Proc. Natl. Acad. Sci. U.S.A.* **83**, 7147 (1986)].
22. $Ru(phen)_2dppz^{2+}$ intercalated itself spans 4 bp; the statistical distribution of complexes on the oligomer generates a larger average binding site.
23. N. Gupta *et al.*, *Angew. Chem. Int. Ed. Engl.* **31**, 1048 (1992).
24. Photocleavage at the intercalation site leads to strand scission with single base 5′ asymmetry. See (*12*).
25. Intimate binding of the phi ligand is essential for productive strand cleavage.
26. The distance between intercalators (the intercalating planes) is given by (the number of base pairs separating the intercalators) × 3.4 Å + 3.4 Å, where the 3.4 Å base pair stacking distance is for B-form DNAs. Thus, intercalation 2 bp in from either end of the 15-bp duplex results in the closest metal-metal distance of 40.8 Å; the most probable distance of 44 Å corresponds to an assembly with one intercalation site 2 bp in from the end of the helix and another intercalation site 1 bp in from the other end.
27. The experiments were performed with a Lambda-Physik excimer-pumped dye laser with excitation at 480 nm and detection at 610 nm. The signal was directed through a monochromator to a Hamamatsu R928 PMT, and decay traces were fit to a multiexponential program. Excitation energies ranged from 0.5 to 1.0 mJ; time resolution was ~10 ns.
28. Steady-state emission experiments were performed on a SLM-Aminco 8000 spectrofluorimeter.
29. The picosecond experiments were performed at the Center for Fast Kinetic Research at the University of Texas at Austin. Laser excitation at 420 nm was provided by a mode-locked Nd:YAG-pumped dye laser. The signal was directed through a 620-nm bandpass filter to a Hamamatsu R928 photomultiplier tube. Decay traces were acquired on a Tracor-Northern TN 7200 multichannel analyzer and deconvoluted from measured instrument response functions.
30. N. J. Turro, *Modern Molecular Photochemistry* (Benjamin-Cummings, Menlo Park, CA, 1978).
31. The driving force is calculated from cyclic voltammetry and spectroscopic measurements, see (*17*). The oxidation potential for $Ru(phen)_2dppz^{2+}$ is −1.56 V versus a standard hydrogen electrode (SHE) and the reduction potential for $Rh(phi)_2phen^{3+}$ is 0.01 V versus SHE.
32. M. Furue, M. Hirata, S. Kinoshita, T. Kushida, M. Kamachi, *Chem. Lett.* **1990**, 2065 (1990); K. Kalyanasundaram, M. Gratzel, Md. K. Nazeeruddin, *J. Phys. Chem.* **96**, 5865 (1992); K. Nozaki, T. Ohno, M. Haga, *ibid.*, p. 10880.
33. C. V. Kumar, J. K. Barton, N. J. Turro, *J. Am. Chem. Soc.* **107**, 5518 (1985); J. K. Barton, J. M. Goldberg, C. V. Kumar, N. J. Turro, *ibid.* **108**, 2081 (1986).
34. The driving force for the photoinduced electron-transfer reaction from $Ru(phen)_3^{2+*}$ to $Rh(phen)_3^{3+}$ is 0.25 V.
35. R. A. Marcus, *Annu. Rev. Phys. Chem.* **15**, 155 (1964); ——— and N. Sutin, *Biochim. Biophys. Acta* **811**, 265 (1985).
36. Electron transfer rates were calculated as in (*1*) and assume an exponential decay with distance. The dielectric constant of DNA is taken to be 78 at large intercharge separations [B. E. Hingerty, R. H. Ritchie, T. L. Ferrell, J. E. Turner, *Biopolymers* **24**, 427 (1985)]. The product of the nuclear frequency factor (ν_n) and the electronic coupling factor when donor and acceptor are in closest contact (κ_e^0) is assumed to be 10^{13} s^{-1} (*1*). The calculated reorganization energy λ is 0.4 eV, neglecting inner-sphere effects (*1*).
37. S. Woitellier, J. P. Launay, C. W. Spangler, *Inorg. Chem.* **28**, 758 (1989).
38. C. C. Moser, J. M. Keske, K. Warncke, R. S. Farid, P. L. Dutton, *Nature* **355**, 796 (1992).
39. We are grateful to C. V. Kumar for helpful discussions and to J. Winkler for expert technical assistance. In addition, J.K.B. thanks the National Institutes of Health (GM49216) and the National Foundation for Cancer Research for their financial support. N.J.T. thanks the National Science Foundation and Air Force Office of Scientific Research for their financial support. We are also grateful to the National Science Foundation for postdoctoral (C.J.M.) and predoctoral (M.R.A.) fellowships as well as the Deutsche Forschungsgemeinschaft (S.H.B.) and the Parsons Foundation (Y.J.). We also thank A. Harriman and S. Atherton of the Center for Fast Kinetic Research, which is supported jointly by NIH and the University of Texas at Austin, for assistance in the single-photon counting measurements.

4 June 1993; accepted 29 September 1993

Picosecond Resolution in Scanning Tunneling Microscopy

G. Nunes Jr.* and M. R. Freeman

A method has been developed for performing fast time-resolved experiments with a scanning tunneling microscope. The method uses the intrinsic nonlinearity in the microscope's current versus voltage characteristics to resolve optically generated transient signals on picosecond time scales. The ability to combine the spatial resolution of tunneling microscopy with the time resolution of ultrafast optics yields a powerful tool for the investigation of dynamic phenomena on the atomic scale.

The scanning tunneling microscope (STM) (*1*) first found wide use in the field of surface science as an atomic-scale probe of topography and electronic structure, but applications of tunneling microscopy now extend from the imaging of such complex molecules as DNA (*2*) to the fabrication of structures out of single atom building blocks (*3*). The success of the STM has also inspired a rapidly growing variety of new scanned probe microscopies based on atomic (van der Waals) forces, magnetic forces, capacitance, and near field optics, to name but a few (*4*). Among these powerful techniques, the STM alone relies on the extremely localized quantum mechanical tunneling of electrons between the sample and the tip and therefore offers the advantage of an extraordinarily high three-dimensional spatial resolution. Although the possibility has long been recognized (*5*), researchers have so far met with limited success in attempting to extend that resolution to the "fourth" dimension, that is, to allow the STM to probe phenomena on atomic *time* scales as well as atomic length scales.

Adding such time resolution to the capabilities of the STM requires that some important obstacles be overcome. Although the intrinsic time scale for tunneling across the junction between the sample and tip in an STM has been estimated to be of order 10 fs or less (*6*), stray capacitance in the wiring and the unavoidable trade-off between signal-to-noise ratio and speed in the external electronics limit the bandwidth in typical instruments to ~30 kHz or less. Similar difficulties arise in the field of ultrafast optics, where the speed of the electronics is no match for femtosecond optical pulses, and it is natural to adapt optical "pump and probe" methods for detecting fast transient signals to time-resolved STM experiments.

In optical experiments, these pump and probe methods often rely on some nonlinearity in the system under study so that the separate response to each of a pair of fast excitations (the "pump" and "probe" pulses) is different from the response when the pulses arrive simultaneously. To overcome the fact that the signal from a lone pump and probe pair will be both too small and too fast to record directly, a continuous train of pulses is applied so that the detec-

IBM Thomas J. Watson Research Center, P.O. Box 218, Yorktown Heights, NY 10598.

*Permanent address: Department of Physics and Astronomy, Dartmouth College, 6127 Wilder Laboratory, Hanover, NH 03755–3528.

tion electronics can integrate the response from many pulse pairs into a signal at low frequencies. The part of the signal that arises from the nonlinearity (which corresponds to the overlap of the pump and probe pulses) is then picked out by using standard phase sensitive techniques. By delaying the arrival time of one of the pulses with respect to the other by an amount t_0 and recording the signal over a range of t_0 values, the fast time response of the system can be mapped out with a resolution roughly equal to the widths of the individual pulses. Hamers and Cahill (*7*) successfully applied such boxcar averaging techniques to the field of scanning probe microscopy. By exploiting the fact that the voltage which appears on the surface of a semiconductor under illumination is a nonlinear function of the light intensity, they were able to use scanning capacitance microscopy to measure the lifetime of photo-excited carriers on the Si(111)-(7 × 7) surface.

A more general approach to time-resolved scanning microscopy, however, must be based on some intrinsic property of the probe itself, rather than of the sample under study. Also, in order to obtain the highest possible spatial resolution, the physical mechanism on which that probe is based must be tunneling. The simplest strategy would be to directly modulate the physical distance between the sample and tip. One need only move the tip closer to the surface for a brief interval to lower the tunneling impedance and sample some fast transient signal. Because this impedance depends exponentially on atomic length scale changes in the tip-sample separation, this mechanically gated detection scheme requires tip motions that are only of order 0.1 nm. Earlier experiments in which a magnetostrictive tip was used to modulate the tunnel junction have successfully demonstrated time resolution in scanning tunneling microscopy on nanosecond scales (*8*). Although the speed of this technique can undoubtedly be improved, the ultimate time resolution of any such junction modulation scheme will always be limited by the difficulty of accelerating the mass of the tip. Here we report on the careful characterization of a broadly applicable time-resolved STM technique which uses no "moving parts," but rather takes advantage of the nonlinear dependence of the tunnel current on the voltage applied between the tip and the sample. This nonlinearity, which depends on the details of the electronic density of states in the sample and tip, is an intrinsic feature of quantum mechanical tunneling, and has been exploited in a variety of mixing and rectification experiments at both optical and microwave frequencies (*9–11*). This approach to pump and probe style STM experiments has enabled us to enter the picosecond regime.

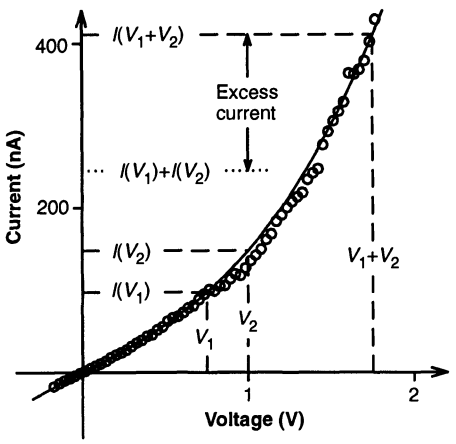

Fig. 1. Measured current versus voltage (*I-V*) characteristic of our STM with a Pt/Ir tip and Au sample (○). During the measurement, the tip-sample separation was held fixed at the separation corresponding to a bias of 20 mV and a quiescent tunneling current of 0.5 nA. For clarity, only the data for positive voltages are shown, although the agreement between the data for negative voltages and the *I-V* characteristic predicted by Simmons (*12*) (solid line) is equally good. The principle of the time-resolved measurements is also illustrated. Because of the nonlinearity in the *I-V* characteristic, the current $I(V_1 + V_2)$ is not equal to sum of the two currents $I(V_1) + I(V_2)$. The difference between these two quantities is shown as the "excess current."

The principle of the experiment is illustrated in Fig. 1, which shows the measured current versus voltage (*I-V*) tunneling characteristics of our STM with a Pt/Ir tip and Au sample (operated in air at room temperature). The solid line is a fit to the form given by Simmons (*12*), who showed that the tunneling current density J through a metal-insulator-metal (MIM) junction at intermediate voltages obeys the general relation:

$$J = \beta(V + \gamma V^3) + O(V^4) \qquad (1)$$

where β and γ depend on the average barrier height and the tip-sample separation. As can be seen from Fig. 1, if a pair of voltage pulses of amplitude V_1 and V_2 are coincident at the junction, the current produced by the whole, $I(V_1 + V_2)$, is greater than the sum of the parts, $I(V_1) + (V_2)$. The "excess" current is the time-resolved signal and is easily discriminated from other components of the total current through lock-in detection. If one of the pulses is applied at time $t = 0$ and the second pulse is applied at $t = t_0$, then, for MIM tunneling as described by Eq. 1, the time-resolved current $I_{tr}(t_0)$ is proportional to:

$$3\beta\gamma \int_x^\infty [V_1(t)]^2 V_2(t - t_0) + V_1(t)[V_2(t - t_0)]^2 \, dt$$

$$x = \begin{cases} t_0 \text{ for } t_0 \geq 0 \\ 0 \text{ for } t_0 < 0 \end{cases} \qquad (2)$$

For tunneling between a metal tip and some other kind of surface (such as a semiconductor), the integrand in Eq. 2 would have a somewhat different form and the time-resolved current itself would be larger because the nonlinearity in MIM tunneling is comparatively weak.

Our experimental arrangement is shown schematically in Fig. 2. The tip of a conventional STM addresses an evaporated Au film in the form of a 50-ohm terminated transmission line, and standard feedback techniques are used to keep a constant quiescent tunneling current. We launch very fast pump and probe voltage pulses onto the transmission line with a pair of GaAs photoconductive switches (*13*) illuminated by a mode-locked picosecond-pulse dye laser. A pair of optical fibers are used to bring the output of the laser onto the vibration-isolated STM platform, and the relative arrival time of the pulses at the tip is controlled by an optical delay line. Because the transient tunnel currents induced by these fast pulses are well outside the bandwidth of our standard current preamplifier, neither the preamp nor the feedback controller can follow them in

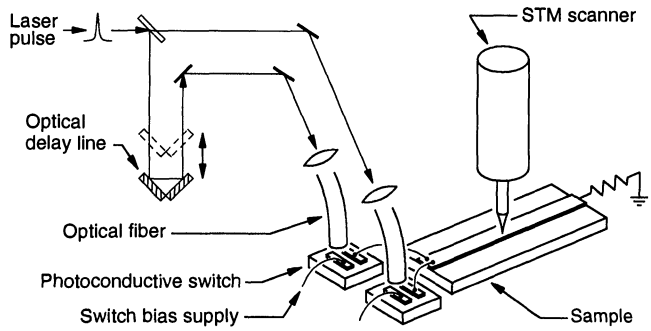

Fig. 2. Schematic illustration of the experimental apparatus. Optical pulses from a mode-locked dye laser are split in two and coupled into a pair of optical fibers. An optical delay line in one of the beam paths allows control of the relative arrival time of the pulses at the fiber outputs. The fibers are used to illuminate a pair of GaAs photoconductive switches that are biased at 10 V. When the light from the fibers allows conduction across one of the switches, a voltage pulse is launched onto the Au transmission line which is addressed by the STM. The 50-ohm resistor attached to the sample prevents the pulses from being reflected back up the transmission line. For clarity, the circuitry used to provide the fixed bias voltage for tunneling is omitted.

"real time." These fast transients are, however, integrated by the preamp to yield a net signal at low frequencies. The part of this signal that corresponds to the overlap of the two pulses at the tunnel junction is picked out by optically chopping the inputs to the fibers at f_1 = 938 Hz and f_2 = 1451 Hz and by detecting the output of the preamp at the sum frequency of 2389 Hz with a lock-in amplifier. The time delay t_0 between the two optical pulses is scanned over a range of 2 ns by adjusting the optical delay line, and the lock-in output is recorded at each setting of t_0 to sweep out the entire time-resolved tunneling signal.

The solid line in Fig. 3 shows the results of such a measurement with a 10-mV dc bias applied between the sample and the tip and with the feedback loop set to maintain a quiescent tunneling current of 500 pA. The two voltage pulses were launched toward the tunnel junction by applying 10 V across the photoconductive switches and illuminating them with 2-ps pulses from the mode-locked dye laser. The amplitude of these voltage pulses at the tunnel junction was on the order of 1 V, as estimated from measurements made with a sampling oscilloscope. The peak evident in Fig. 3 represents the actual time-dependent response of the STM to the overlapping voltage pulses. The STM was held fixed above a single point on the surface during these measurements. The zero of time was chosen to correspond to the instant at which the peaks of the two pulses coincide, and a small, time-independent background has been subtracted from the data. This background signal arises from capacitive coupling to the tip and appears to be independent of tip-sample separation out to large (micrometer) separations. The time-resolved signal, on the other hand, is very sensitive to the tip-sample distance, as expected from the strongly distance-dependent tunneling interaction that gives the STM its high spatial resolution. It drops below the detection limit of our electronics if the tip is backed off as little as 1 nm from the surface, which allows us to discriminate completely against spurious signals.

In order for the time-resolved STM to be useful, of course, it must be possible to relate the shape of the time-resolved current I_{tr} to the time dependence of the underlying processes. In the present case, the time-domain shape of the voltage pulses depends on the behavior of the photoconductive switches. The rise time of the pulses is essentially determined by the 2-ps width of the optical pulses. The decay time of the pulses depends on the carrier recombination time in the GaAs and, for these switches deposited on semi-insulating bulk material, is on the order of 100 ps. Because the decay time of the voltage pulses is so much longer than their rise time, we may ignore the latter and approximate the time dependence of the pulses by a step function followed by a simple exponential decay:

$$V(t) \propto \begin{cases} 0 & \text{for } t < 0 \\ e^{-t/\tau} & \text{for } t \geq 0 \end{cases} \quad (3)$$

The expected I_{tr} can be found by substituting V_1 and V_2 of this form into Eq. 2 and performing the integration analytically. Impedance mismatches in the system lead to some back-reflection (ringing) of the pulses, which we have approximated through the mathematical convenience of multiplying one of the pulses by a cosine function. The dashed line in Fig. 3 is the result of a least-squares fit in which the decay constant τ and the overall signal amplitude, as well as the frequency and phase of the cosine function, were taken as free parameters. As can be seen from Fig. 3, the agreement between the data and the behavior predicted by Eqs. 2 and 3 with τ = 114 ps is excellent. The amplitudes of the individual voltage pulses, as extracted from the fit, were 0.8 and 1.5 V.

Physically connecting the photoconductive switches to the sample allowed us to thoroughly characterize this method for time-resolved scanning tunneling microscopy. The actual instrument, however, is configured to allow entirely "noncontact" experiments. Rather than propagating the probe pulse onto the sample, we use a small wire to capacitively couple it directly to the microscope's tip. The microscope can then serve as a high impedance (nonperturbative) probe of any transient electrical signal in the sample. As an example of such a noncontact measurement, Fig. 4 shows the signal obtained from using the time-resolved STM to sample a fast logic pulse propagating along the Au transmission line. Similar time resolution has recently been obtained by Hou *et al.* (*14*) using a novel scanning microscope based on electrostatic forces which, while fast, cannot offer the high spatial resolution allowed by tunneling microscopy. For comparison purposes, Fig. 4 also shows the pulse shape as obtained with a high-speed sampling oscilloscope. The broadening apparent in this case is an artifact of the wiring used to connect the signal to the external detector.

The implications of this "noncontact" experiment are far reaching. Indeed, the voltage pulse applied to the Au surface may be thought of as a stand-in for almost any optically induced modification of a sample's surface electronic density of states. In particular, such optically excited phenomena as photovoltage on semiconductor surfaces, gap reduction in nonequilibrium superconductors, and photoconductivity in organic molecules are all examples from the wide class of systems in which important new investigations are made possible by the combination of high spatial and fast time resolution. These experiments show that it is possible to use the STM to probe these phenomena on picosecond time scales, and represent substantial progress toward the goal of probing atomic-scale dynamics in all four (space-time) dimensions.

Note added in proof: We have lately become aware of a similar experiment by S. Weiss *et al.* (*15*).

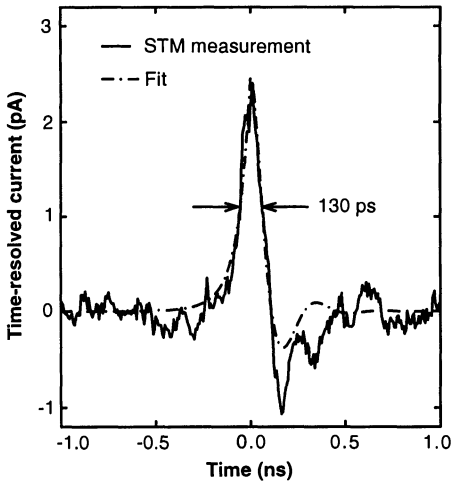

Fig. 3. Time-resolved tunneling current obtained using the arrangement shown in Fig. 2. The data are indicated by the solid line. The dashed line is a fit to the data by using Eq. 2 and by assuming a simple exponentially decaying form for the optically launched voltage pulses. To account for the ringing due to impedance mismatches in the system, one of the pulses has been multiplied by a cosine function.

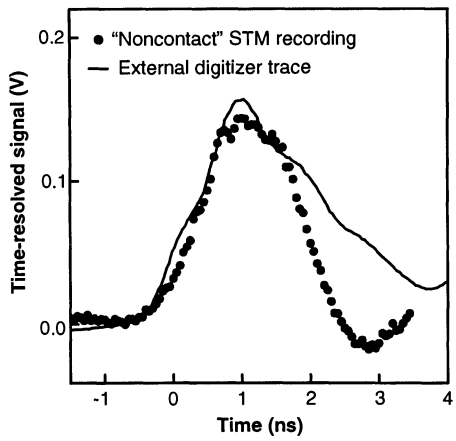

Fig. 4. Time-resolved STM measurement of a fast logic pulse. This measurement was made with a "noncontact" implementation of the microscope in which the probe pulse is capacitively coupled onto the tip (●). The solid line shows the pulse shape as obtained with a high-speed digitizing oscilloscope. The broadening apparent in this digitized trace is an artifact of the connection to the oscilloscope.

REFERENCES AND NOTES

1. G. Binnig, H. Rohrer, Ch. Gerber, E. Weibel, *Appl. Phys. Lett.* **40**, 178 (1982); G. Binnig and H. Rohrer, *IBM J. Res. Dev.* **30**, 355 (1986), and references therein.
2. M. Amrein, A. Stasiak, H. Gross, E. Stoll, G. Travaglini, *Science* **240**, 514 (1988).
3. D. M. Eigler and E. K. Schweizer, *Nature* **344**, 524 (1990).
4. See, for example, H. K. Wickramasinghe, Ed., volume 241 of the *AIP Conference Proceedings* (American Institute of Physics, New York, 1991).
5. N. M. Amer, A. Skumanich, D. Ripple, *Appl. Phys. Lett.* **49**, 137 (1986).
6. P. H. Cutler, T. E. Feuchtwang, T. T. Tsong, H. Nguyen, A. A. Lucas, *Phys. Rev. B* **35**, 7774 (1987).
7. R. J. Hamers and D. G. Cahill, *Appl. Phys. Lett.* **57**, 2031 (1990); *J. Vac. Sci. Technol.* **B9**, 514 (1991).
8. M. R. Freeman and G. Nunes Jr., *Appl. Phys. Lett.*, in press.
9. L. Arnold, W. Krieger, H. Walther, *ibid.* **51**, 786 (1987).
10. G. P. Kochanski, *Phys. Rev. Lett.* **62**, 2285 (1989).
11. R. Möller *et al.*, *J. Vac. Sci. Technol.* **B9**, 506 (1991).
12. J. G. Simmons, *J. Appl. Phys.* **34**, 238 (1963).
13. D. H. Auston, *Appl. Phys. Lett.* **26**, 101 (1975).
14. A. S. Hou, F. Ho, D. M. Bloom, *Electron. Lett.* **28**, 2302 (1992).
15. S. Weiss *et al.*, *Appl. Phys. Lett.* **63**, 2567 (1993).

16. We thank N. M. Amer, S. von Molnar, R. S. Germain, and R. M. Feenstra for careful readings of the manuscript.

2 August 1993; accepted 28 September 1993

Evidence for Large Upward Trends of Ultraviolet-B Radiation Linked to Ozone Depletion

J. B. Kerr* and C. T. McElroy

Spectral measurements of ultraviolet-B radiation made at Toronto since 1989 indicate that the intensity of light at wavelengths near 300 nanometers has increased by 35 percent per year in winter and 7 percent per year in summer. The wavelength dependence of these trends indicates that the increase is caused by the downward trend in total ozone that was measured at Toronto during the same period. The trend at wavelengths between 320 and 325 nanometers is essentially zero.

In 1974 it was proposed (*1*) that the continued use of chlorofluorocarbons (CFCs) would lead to a decrease in the amount of stratospheric ozone. This prediction led to concerns about possible detrimental effects on human health and other biological systems that might follow from the increased levels of ultraviolet-B (UV-B) radiation at the Earth's surface because of the decrease in the stratospheric ozone column. The first conclusive evidence for a downward trend in ozone levels was reported (*2*) in 1985 where springtime values of ozone over the Antarctic were observed to have declined by 40% between 1975 and 1984. More recently, negative trends in ozone levels at other locations have been reported (*3–5*) and their seasonal and geographical dependencies have been determined. Extensive field studies in the Antarctic (*6*) and Arctic (*7*) have associated the loss of ozone with high levels of chlorine in the stratosphere.

Definitive measurements of a long-term trend in UV-B radiation as a result of the decline in ozone levels at mid-latitudes have been difficult to obtain. Measurements have shown that short-term, day-to-day fluctuations of UV-B radiation vary as expected with changes in column ozone amount both in the Northern (*8*) and Southern (*9*) hemispheres as well as under the Antarctic ozone hole (*10, 11*). However, attempts to detect long-term trends in UV-B radiation from existing data records have been inconclusive and controversial. For example, an analysis (*12*) of data from a network of broad-band Robertson-Berger meters in the United States showed a negative trend in UV-B radiation levels at a time when ozone levels were known to be decreasing.

The detection of a long-term change of UV-B radiation is considerably more difficult than the measurement of the long-term decline of ozone levels. One reason is that the intensity of UV-B radiation at the Earth's surface depends on many factors other than stratospheric ozone, including clouds, aerosols, haze, pollutants and ground albedo. Periodic or long-term changes of any of these variables will influence trend results derived from the analysis of UV-B measurements. It is essential that instruments making the measurements be well characterized and that a good calibration of instrumental response be maintained for a long period of time. Because of the difficulty of the measurement, UV-B data are sparser, available for a shorter time interval, and are poorer in quality than the ozone record, making trend analysis uncertain.

In this paper we report spectroradiometric UV-B measurements made at Toronto (44°N, 79°W) between 1989 and 1993. Our results are from Brewer instrument number 14, one of the triad of independently calibrated instruments maintained at Toronto as the Canadian total ozone reference. The Brewer instrument measures the intensity of UV-B radiation falling on a horizontal diffusing surface. Measurements are made at wavelength intervals of 0.5 nm between 290 and 325 nm with a resolution of about 0.5 nm. Each spectral measurement consists of the average of a forward and backward wavelength scan, which takes about 8 min to complete. Measurements are made between once and twice each hour throughout the day from sunrise to sunset.

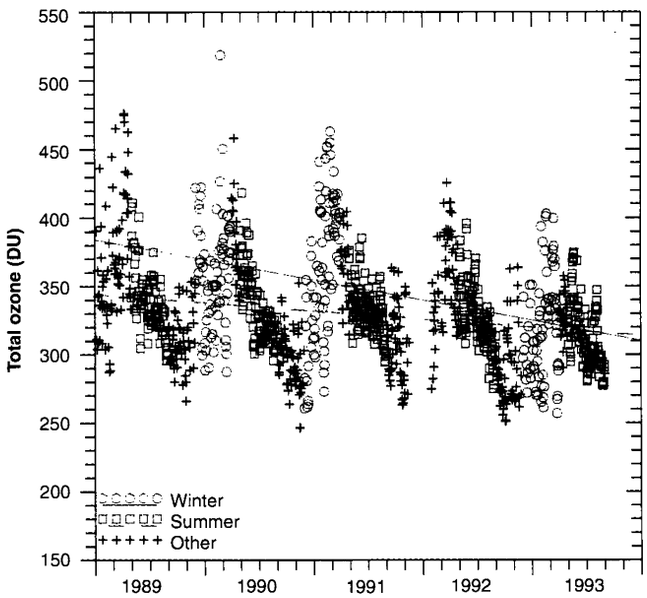

Fig. 1. Record of daily ozone measurements between 1989 and 1993. The straight lines are the best-fit linear trends through the winter (December to March; −4.1% per year) and summer (May to August; −1.8% per year) data points with the annual cycle removed.

Environment Canada, Atmospheric Environment Service, 4905 Dufferin Street, Downsview, Canada M3H5T4.

*To whom correspondence should be addressed.